Molecular dynamics study of vibrational energy relaxation of CN− in H2O and D2O solutions: An application of path integral influence functional theory to multiphonon processes

ARTICLE *in* THE JOURNAL OF CHEMICAL PHYSICS · SEPTEMBER 1999

Impact Factor: 2.95 · DOI: 10.1063/1.479799

2 AUTHORS, INCLUDING:

Motoyuki Shiga
Japan Atomic Energy Agency
88 PUBLICATIONS **1,438** CITATIONS

Molecular dynamics study of vibrational energy relaxation of CN^- in H_2O and D_2O solutions: An application of path integral influence functional theory to multiphonon processes

Motoyuki Shiga and Susumu Okazaki[a)]
Department of Electronic Chemistry, Tokyo Institute of Technology, 4259 Nagatsuta, Midori-ku, Yokohama 226-8502, Japan

(Received 8 December 1998; accepted 25 June 1999)

Vibrational energy relaxation of a cyanide ion in the aqueous solutions has been investigated. Both the solute (CN^-) and the solvent (H_2O or D_2O) were treated quantum mechanically based upon the path integral influence functional formalism assuming a harmonic oscillator bath. Single and multiphonon spectral densities were evaluated numerically from the normal modes of the solvent, i.e., the bath phonons, and the linear and nonlinear coupling constants between the C–N stretching coordinate and the phonons for 30 different quenched and instantaneous solvation structures generated by molecular dynamics calculations. The method combined with the normal mode analysis successfully presented not only the time constant of the relaxation but also information about what sorts of the solvent bath modes are responsible for the relaxation process. We show that two-phonon process caused by the nonlinear coupling between the C–N stretching mode and two bath phonons are shown to be mostly responsible for the present system. It is found, too, that the coupling of the system with two bath rotational libration modes and the coupling with a bath bending mode and a bath rotational libration mode are dominant in the relaxation process in an H_2O solution, while, in a D_2O solution, the coupling with the bath bending mode and bath rotational libration mode is most important. The normal modes that represent large motion of the water molecules inside the first and second solvation shells of the cyanide ion are particularly significant for the relaxation. © *1999 American Institute of Physics.* [S0021-9606(99)50136-0]

I. INTRODUCTION

In spite of the recent progress of computers, it is still hopeless to investigate many-body quantum dynamics in condensed phase rigorously. However, for most chemical reactions and state-to-state transition dynamics of chemical species, the system coordinate of interest, which is local in space, can be separated from a large number of other solvent coordinates. Then, one possible way to avoid the difficulty is to introduce an approximation for the solvent, keeping the rigorous treatment for the system of interest. From this standpoint, one of the theoretical framework, that can describe the quantum dynamics of the system of interest interacting with its surroundings is the influence functional theory (IFT).[1,2] The idea of IFT is to divide the whole system into the system of interest and the environment and to concentrate on the reduced density matrix of the system of interest. The environmental degrees of freedom can be integrated out algebraically if they are assumed as a set of harmonic oscillators. After the integration, the effect of the environment on the time evolution of the reduced density matrix of the system is formally determined by the functional of the system variable itself, the influence functional. Thus, we obtain an equation composed of only the system variable. Since the time evolution of the system and environment are dependent upon each other, the expression of the influence functional is, in general, nonlocal in time; the multiple integral form of the influence functional represents the retarding effect of the external field imposed upon the system. The influence functional involves the effect of the environment on the system dynamics and dynamical change of the environment caused by the system influences back on the system dynamics.

Thus, the IFT is a rigorous theory that treats the potential fluctuation of the system exerted by the solvent. The IFT may be expected to have a wide range of applications to chemical problems in the condensed phase such as quantum transition dynamics and the solvation effect on the reaction rates.

In our previous paper, perturbative influence functionals have been obtained for the system nonlinearly coupled to a set of harmonic bath oscillators,[3] where nonlinear cross couplings of bath modes were considered. The functional can be used to describe transition dynamics of a quantum system caused by multiphonon processes in the condensed phase. In the present work, the theory has been applied to vibrational energy relaxation of a real chemical system, cyanide ion in the aqueous solutions, based upon molecular dynamics approach. According to our preliminary calculation,[4] the method, with the aid of normal mode analysis for liquids, was found to be promising. Here, we show a full report of this application study.

Vibrational energy relaxation of a system in the solution has been one of the major subjects of current physical chemistry, since the rate of energy exchange between the system

a)Author to whom correspondence should be addressed. Electronic mail: okazaki@echem.titech.ac.jp

and its surrounding solvent must be closely related to pathways of condensed phase chemical reactions. In this sense, it is of general interest to study what sort of mechanism underlies in the vibrational energy transfer process. In fact, experimental progress in this area has been accelerated by the development of time-resolved pump-probe spectroscopy, which has provided an access to picosecond or faster time scale processes. For example, vibrational energy relaxation has extensively been investigated for various solutions.[5–11] Recently, the experiments have been focused on polar diatomic molecules and ions in polar solvents since the mechanism of vibrational relaxation is very interesting when the solvent strongly couples to the solute.[12,13] However, from the experiment only, it is very difficult to get information about the energy transfer pathway to and from the translational, rotational, and vibrational degrees of freedom of the solvent molecules. Thus, it is very interesting to investigate the dissipation mechanism of the energy to the solvent molecules by computer simulation. In fact, many theoretical studies have been presented to solve this problem.[14–56] In particular, a few numerical calculations of the vibrational relaxation rate based upon Fermi's golden rule have been reported, extracting the autocorrelation function of force exerted on the solute molecule from a classical molecular dynamics (MD) trajectory.[56] However, neglect of the quantum mechanical effect in the above studies is fatal when the energy gap of the solvent as well as solute eigenstates are much greater than k_BT. A quantum correction assuming harmonic oscillators bath does not work well for the multiphonon processes, either.[3,54]

Here, for the CN^- ion in the aqueous solution, both the system of interest and the solvent have been quantum mechanically treated, taking account of intrinsic quantal nature of high-frequency vibrations, since the vibrational modes of water molecules as well as the cyanide ion are larger than $k_BT/hc \sim 200\,\mathrm{cm}^{-1}$ at room temperature. The reason why this system attracts a number of experimentalists and theorists is that multiphonon coupling must play a predominant role in the relaxation process since there are no solvent water modes whose frequency $\tilde{\omega}_s$ is around that of the solute C–N stretching mode 2080 cm^{-1}. Further, for the diatomic solute such as CN^-, intermolecular energy transfer between the solute and the solvent must dominate the relaxation process, since energy flow by the intramolecular V–V transfer does not exist.

As shown later, it is convenient to introduce ''spectral densities'' in order to investigate the effect of environment on the dynamics of the system. The spectral densities characterize the interplay of fluctuation and dissipation representing both the number of oscillators with a given frequency present in the environment and the interaction between the oscillators and the system. Based upon the multiphonon spectral densities recently obtained by us,[3] we can analyze not only the energy relaxation time but also what sorts of solvent modes contribute to the relaxation of the CN^- ion in the H_2O and D_2O solutions.

The strategy of the present study to investigate the vibrational energy relaxation can be described by the following several steps: (1) Conventional molecular dynamics calculation at the room temperature 300 K that provides initial configurations of the solution for the quench process of the second step; (2) quench of the solution to the local potential minimum; (3) normal mode analysis for the solvent $\{q_k\}$; (4) evaluation of the linear and nonlinear coupling constants by numerical differentiation at each solvation structure; (5) calculation of the spectral densities and time-dependent transition probability based upon the golden rule formula that are expressed by the coupling constants, and, finally; (6) analysis of the normal modes that has a large contribution to the transition probability. The above procedure has also been done for the instantaneous normal mode, skipping the second step.

Normal modes in liquids have been investigated extensively.[57–68] In particular, instantaneous normal modes have been analyzed in detail to understand the dynamics of molecules in the liquids. This presents a useful classical approximation to describe vibrational relaxation in the liquids.[60–65] These are all promising to be a powerful tool in the study of liquid state molecular dynamics. However, in this study, we are concerned only with primitive normal modes, i.e., quenched and instantaneous normal modes, since the purpose of the present calculation is to demonstrate an efficacy and usefulness of our theory for the multiphonon process. There might be better choices for liquid state harmonic modes. In any case, here, 30 quenched and 30 instantaneous structures have been obtained by classical molecular dynamics calculations for one CN^- ion, one Na^+ ion and 254 H_2O (or D_2O) molecules in the periodic boundary condition. Frequencies of the bath oscillators and the linear and nonlinear coupling constants have been evaluated for each quenched and instantaneous structure. We show that the calculated relaxation time of CN^- in a vibrationally excited state was in moderate agreement with the experimental result,[13] taking account of the two-phonon process, i.e., nonlinear coupling of two bath modes.

II. THEORY AND CALCULATION

A. Multiphonon processes

Before stepping into details, it may be of benefit to the readers to summarize several possible origins of multiphonon processes in the condensed phase. Vibrational energy relaxation can be caused by linear coupling with the solvent molecules as well as various kinds of nonlinear interactions involved in the total system. Let us express the total Hamiltonian as

$$H = H_s(x) + H_b(\{q_k\}) + H_i(x,\{q_k\}), \tag{1}$$

where x is the system coordinate and $\{q_k\}$ represents a set of harmonic bath modes. H_s, H_b, and H_i are the Hamiltonian of the system, bath, and interaction between them. In the present case, the one-dimensional system Hamiltonian is expressed by

$$H_s(x) = -\frac{\hbar^2}{2m_s}\frac{\partial^2}{\partial x^2} + V_s(x), \tag{2}$$

and the assumed harmonic bath Hamiltonian by

$$H_b(\{q_k\})=\sum_{k=1}^{N}\left(-\frac{\hbar^2}{2m_k}\frac{\partial^2}{\partial q_k^2}+\frac{1}{2}m_k\omega_k^2 q_k^2\right). \tag{3}$$

The system–bath interaction Hamiltonian is in a general form,

$$H_i(x,\{q_k\})=H_i^{(\mathrm{LL})}(x,\{q_k\})+H_i^{(\mathrm{NL})}(x,\{q_k\}) +H_i^{(\mathrm{LN})}(x,\{q_k\})+H_i^{(\mathrm{NN})}(x,\{q_k\}), \tag{4}$$

where

$$H_i^{(\mathrm{LL})}(x,\{q_k\})=\sum_{k=1}^{N}C_k^{(1)}xq_k, \tag{5}$$

$$H_i^{(\mathrm{NL})}(x,\{q_k\})=\sum_{k=1}^{N}C_k^{(2)}x^2q_k+\sum_{k=1}^{N}C_k^{(3)}x^3q_k+\cdots, \tag{6}$$

$$H_i^{(\mathrm{LN})}(x,\{q_k\})=\sum_{k=1}^{N}\sum_{l=1}^{N}C_{kl}^{(1)}xq_kq_l +\sum_{k=1}^{N}\sum_{l=1}^{N}\sum_{m=1}^{N}C_{klm}^{(1)}xq_kq_lq_m+\cdots, \tag{7}$$

and

$$H_i^{(\mathrm{NN})}(x,\{q_k\})=\sum_{k=1}^{N}\sum_{l=1}^{N}C_{kl}^{(2)}x^2q_kq_l+\cdots \tag{8}$$

are linear–linear, nonlinear–linear, linear–nonlinear, and nonlinear–nonlinear components, respectively, of the Taylor expansion of H_i with respect to x and q_k. The indices L and N in the interaction Hamiltonian H_i's stand for linear and nonlinear couplings, respectively, with respect to x and $\{q_k\}$. Here, m_s, m_k, ω_k, and $V_s(x)$ denote the mass of the system, the mass of the kth bath mode, the frequency of the kth bath mode, and the potential of the system, respectively. Here, zeroth-order terms in the expansion of H_i with respect to the bath coordinates q_k, which are simply proportional to x, x^2, x^3…, are included in $V_s(x)$. On the other hand, the zeroth-order expansion term with respect to the system coordinate x, which is a function of $\{q_k\}$, is excluded from the equation according to the harmonic bath approximation. The coefficients C's represent the coupling constants between the system and the harmonic bath.

To our knowledge, there has been little systematic argument of which of the above anharmonic couplings is essential in vibrational relaxation, except for the simple estimation by Egorov and Skinner.[49] For this reason, it is interesting to calculate the values of the anharmonic coupling constants directly based upon actual solvation structures of the real system. In the present case, the system coordinate x is assigned to the vibrational coordinate of the cyanide ion, and the bath coordinates $\{q_k\}$ to the normal modes of solvent water and translational and rotational degrees of freedom of the ion.

First, it is convenient to assume a harmonic oscillator, $V_s(x)=\frac{1}{2}m_s\omega_s^2x^2$, for the C–N stretching. This approximation must be valid for the vibrational relaxation of molecules, since the system potential may be assumed to be intrinsically quadratic with respect to x when the system was initially in a low vibrationally excited state such as the first excited state and is finally found in the ground state. If highly excited states are concerned, anharmonicity in $V_s(x)$ must be taken into account. Second, in the present calculation, terms higher than quadratic with respect to the bath coordinates were neglected, i.e. $C_{klm}^{(u)}=0$,..., just because the calculation including all these terms is too heavy. However, we believe that this approximation does not affect much the following discussions.

As discussed by Egorov and Skinner,[49] there are two different pathways for the multiphonon process. Let us consider the case that the system potential $V_s(x)$ is harmonic as assumed above. Then, transition between the system eigenstates must be accompanied by absorption and emission of the ''system phonons.'' The first-order perturbation theory with respect to H_i's in Eq. (4) gives Fermi's golden rule. In this case, $H_i^{(\mathrm{LL})}$ gives the process of exchanging one system phonon $\hbar\omega_s$ for one bath phonon $\hbar\omega_k$. Similarly, $H_i^{(\mathrm{NL})}$ gives the process of exchanging system phonons $u\hbar\omega_s$ for a bath phonon $\hbar\omega_k$, where u corresponds to the order of power in the coupling $C_k^{(u)}x^uq_k$. In the present article, these processes are referred to as single-phonon processes, since only a single bath phonon is involved. On the other hand, $H_i^{(\mathrm{LN})}$ gives the process of exchanging a system phonon $\hbar\omega_s$ for several bath phonons $\hbar\omega_k+\hbar\omega_l+\cdots$, and $H_i^{(\mathrm{NN})}$ gives the process of exchanging several system phonons $u\hbar\omega_s$ for bath phonons $\hbar\omega_k+\hbar\omega_l+\cdots$. The number of bath phonons involved in the processes is represented by the number of bath indices in the coupling constants $C_{kl}\cdots$. For example, the term $C_{kl}^{(u)}x^uq_kq_l$ contributes to two-phonon processes, $C_{klm}^{(u)}x^uq_kq_lq_m$ to three-phonon processes, and so on. These processes are the first pathway in the multiphonon processes. Next, the second way to obtain multiphonon processes comes from the higher-order perturbations with respect to H_i's, i.e.; beyond Fermi's golden rule. The nth-order perturbation represents the transition through $n-1$ virtual intermediate states. In each transition between the intermediate states (and also between the intermediate state and the initial or final state), emission and absorption of the system and bath phonons occurs according to the coupling H_i. In this case, thus, the multiphonon processes are brought about not only by the coupling $H_i^{(\mathrm{LN})}$ and $H_i^{(\mathrm{NN})}$ but also by $H_i^{(\mathrm{LL})}$ and $H_i^{(\mathrm{NL})}$.

In our previous study,[3] we obtained formulations of time-dependent transition probability for both mechanisms of the multiphonon processes. The former is obtained by the path integration after the cumulant expansion of the influence functional to the first order. The latter is evaluated by the exact path integration for the full influence functional. Thus, in principle, the both mechanisms may be analyzed based upon the present path integral influence functional theory. As a first step, in the present study, the former multiphonon process is investigated. This process is characterized by the multiphonon spectral densities, which is shown in our previous work.[3]

B. Molecular dynamics calculation

First, a standard classical MD calculation has been performed for the system composed of a single CN^- ion, a Na^+

ion, and 254 H_2O molecules in the cubic cell in the periodic boundary condition. The density was 1 g/cm^3. At this point, all the molecules were modeled by rigid bodies subject to Euler's equations of motion. The potential model by Ferrario *et al.*[69] was adopted for Na^+ and CN^- ions and the TIP4P potential model[70] for H_2O and D_2O molecules. These models are composed of the intermolecular site–site interaction of Lennard-Jones and Coulombic types. The Lorentz–Berthelot combination rule was applied for the parameters of different kinds of Lennard-Jones potential sites. The interaction between the molecules whose distance is longer than one-half of the cell length, 19.7 Å, was truncated. The temperature was set to be 300 K using Nosé thermostat. The production run was executed for total of 300 000 steps with the time step of $\Delta t = 0.5$ fs. Thirty molecular configurations were sampled every 5 ps along the trajectory. The configurations were supplied, first, for the instantaneous normal mode analysis. Further, starting from each instantaneous structure, 30 quenched configurations at local potential minima were obtained by lowering the MD temperature to 0 K. The bond lengths of CN^- and H_2O (or D_2O) were fixed in the quenching procedure just to save CPU time, since the fixed and quenched structures with respect to the intramolecular degrees of freedom gives practically the same normal mode coordinates and the coupling constants. The fluctuation of the equilibrium C–N bond length was less than 0.01 Å and that of O–H (and O–D) was even smaller. These do not affect the evaluation of the normal modes and the coupling constants.

Further, the same quenched structures were used for the normal mode analysis of the D_2O solution; 254 H_2O molecules were simply replaced by 254 D_2O molecules. This is not only because the quenched solvation structures is almost the same between H_2O and D_2O solutions, but also because the isotope effect of solvent water can be examined with all other conditions being the same. The counter ion Na^+ was located at various positions from CN^- among the quenched and instantaneous configurations.

C. Normal modes of water molecules

For each quenched and instantaneous structure, Hessian and kinetic matrix elements were evaluated by numerical differentiation of the potential energy with respect to Cartesian coordinates, Eulerian angles, and also *intramolecular vibrational coordinates* of the ions and the solvent molecules. The vibrational coordinates of H_2O and D_2O molecules were determined from an *ab-initio* calculation based upon B3LYP density functional theory using a 6-31+G* basis set. The vibrational frequencies of isolated H_2O D_2O molecules were set to be 1595 (1178), 3657 (2666), and 3756 (2789) cm^{-1} for bending, symmetric stretching, and antisymmetric stretching modes, respectively. The normal modes were calculated by the diagonalization of 2294 degrees of freedom for the total bath, i.e., 254 (H_2O or D_2O) $\times 9$ $+1(Na^+)\times 3+1(CN^-)\times 6-1$ (CN^- vibration). Reduced coordinates were adopted such that $m_s=1$ and $m_k=1$, where m_s and m_k are reduced masses of the system and bath, respectively, although we show m_s and m_k explicitly in the formulas below for clarity. All the normal mode frequencies for the quenched structures were real except for three of the total system. The imaginary-frequency modes appearing in the instantaneous normal modes were neglected.

D. System vibrational potential of CN^-

The system potential V_s may be given by

$$V_s(x)=\tfrac{1}{2}m_s\tilde{\omega}_s^2x^2, \tag{9}$$

as assumed above, where $\tilde{\omega}_s=\sqrt{\omega_s^2+\Delta\omega_s^2}$ is the frequency of the system in the solutions. Here, ω_s is the frequency of the isolated CN^- molecule, which has been determined in the following way. First, an *ab-initio* calculation was done both for CN^- and CN^+ ions based upon the B3LYP density functional theory using a 6-31+G* basis set. Then the calculated frequency for CN^- was scaled by experimental frequency for CN^+ divided by the calculated value of CN^+ to give the frequency of the isolated CN^-, 2067 cm^{-1}. $\Delta\omega_s$ is the second derivative of the interaction potential energy of the CN^- molecule with the solvent water, which has been determined from molecular dynamics potential functions. Since $\Delta\omega_s$ was evaluated for the solvation structure at $\{q_k\}=0$, it may be referred to as the ''static'' deviation of the potential energy. This corresponds to the zeroth-order expansion term with respect to the bath coordinates. This must be distinguished from the effect by the term such as $C_k^{(2)}x^2q_k$ in Eq. (4), which may be called ''dynamic'' deviation of the potential energy, since they are dependent upon the solvent coordinates $\{q_k\}$. The latter contributes to the vibrational energy relaxation.

E. Coupling constants between system and bath

Coupling constants in the interaction Hamiltonian H_i's in Eqs. (5)–(8) were obtained from potential derivatives at each quenched/instantaneous configuration. For example, $C_{kl}^{(2)}$ in $H_i^{(\mathrm{NN})}$ was calculated by

$$C_{kl}^{(2)}=\frac{1}{2}\left.\frac{\partial^4V}{\partial^2x\,\partial q_k\,\partial q_l}\right|_{x=\{q_k\}=0}, \tag{10}$$

where V is the potential of the total system, including the bath. In order to calculate the coupling constants, first, algebraically obtained potential energy derivatives with respect to Cartesian coordinates, molecular orientation, and vibrational degrees of freedom of the solvent molecules have been evaluated. After transforming these derivatives to the normal mode space, they were numerically differentiated with respect to x. In the evaluation of the Hessian matrix and the coupling constants, we have modeled that the potential may be given by the superposition of the site–site interaction on the intramolecular vibrational potential. In the calculation of the potential derivatives, further, we assumed that the sites of pseudopoint charges in the CN^- ion model move in accordance with the C atom, and the site of pseudocharge of the TIP4P model for H_2O and D_2O molecules moves with the O atom.

F. Survival probability

We will show in Sec. III that, as a result, the coupling constants $C_k^{(u)}$ and $C_{kl}^{(u)}$ with $u \geqslant 2$ have a negligible contribution to the vibrational relaxation of the present system, the CN^- ion in water. Thus, we will take into account only $C_k^{(1)}$ and $C_{kl}^{(1)}$ in the calculation of the spectral densities and relaxation time. Then, the interaction Hamiltonian in Eq. (4) is linear in the system coordinate x. In the stochastic theory, this corresponds to an approximation that the force f exerted on the system is a Gaussian process,[2] which comes from the fact that the product of x and f has a dimension of energy.[71] Goodyear and Stratt[61,62] showed that instantaneous normal modes do not necessarily lead to a Gaussian process, even when they are linearly coupled to the system, since anharmonic equilibrium distribution of instantaneous liquid configurations causes non-Gaussian behavior. However, as a first approximation, we neglect these non-Gaussian effects. Based upon this approximation, time-dependent survival probability at an eigenstate of H_s, e.g., ϕ_i, can be calculated using the Pauli's formula,

$$P[\phi_i \rightarrow \phi_i] = \exp\left(-\sum_{f \neq i} R[\phi_i \rightarrow \phi_f] t \right). \tag{11}$$

Here, we defined Fermi's golden rule transition rate,

$$R[\phi_i \rightarrow \phi_f] = \frac{2}{\hbar^2} \mathrm{Re}\left[\int_0^\infty ds\, G(s) |\langle \phi_i | x | \phi_f \rangle|^2 \times \exp\{ i(\nu_i - \nu_f) s \} \right], \tag{12}$$

with $\hbar \nu_n$ the eigenvalue of the state ϕ_n. This is the expression for the probability that the system was initially at the state ϕ_i and is still found at ϕ_i at $t=t$. We have defined, too, that[3]

$$G(s) = \int_{-\infty}^{\infty} d\omega [\mathcal{T}_{\alpha[1]}(\omega) + \mathcal{T}_{\beta[1]}(\omega) + \mathcal{T}_{\beta[2]}(\omega)] \times [z(\omega)\cos(\omega s) - i \sin(\omega s)], \tag{13}$$

where

$$\mathcal{T}_{\alpha[1]}(\omega) = \sum_{k=1}^{N} \frac{\{C_k^{(1)}\}^2}{2 m_k \omega_k} \delta(\omega - \omega_k),$$

$$\mathcal{T}_{\beta[1]}(\omega) = \sum_{k=1}^{N} \sum_{l=1}^{N} \frac{\hbar \{C_{kl}^{(1)}\}^2 (z(\omega_k) + z(\omega_l))}{(2 m_k \omega_k)(2 m_l \omega_l)} \times \delta(\omega - \omega_k - \omega_l), \tag{14}$$

$$\mathcal{T}_{\beta[2]}(\omega) = \sum_{k=1}^{N} \sum_{l=1}^{N} \frac{\hbar \{C_{kl}^{(1)}\}^2 (-z(\omega_k) + z(\omega_l))}{(2 m_k \omega_k)(2 m_l \omega_l)} \times \delta(\omega - \omega_k + \omega_l),$$

and

$$z(\omega) = \coth(\hbar \omega / 2 k_B T). \tag{15}$$

T is the temperature of the bath and k_B is the Boltzmann constant. We call $\mathcal{T}_{\alpha[1]}(\omega)$, $\mathcal{T}_{\beta[1]}(\omega)$, $\mathcal{T}_{\beta[2]}(\omega)$ the single-phonon spectral density, two-phonon sum-frequency spectral density, and two-phonon difference-frequency spectral density, respectively. First, $\mathcal{T}_{\alpha[1]}(\omega)$ is a function of frequency ω, which measures the total strength of the bath phonons with frequency ω. In the same manner, $\mathcal{T}_{\beta[1]}(\omega)$ and $\mathcal{T}_{\beta[2]}(\omega)$ characterize the total strength of the ''imaginary'' bath phonons generated by the two ''real'' bath phonons.

In order to clarify what sorts of solvent modes are responsible for the relaxation, it is informative to classify the normal modes into translational libration (T), rotational libration (R), intramolecular bending (B), and intramolecular stretching (S) modes of water by the frequencies.[72] In other words, we may define the ''partial spectral densities'' for T, R, B, and S modes. For example, the two-phonon sum-frequency RB spectral density may be defined by

$$\mathcal{T}_{\beta[1]}^{RB}(\omega) = \sum_{k \in R} \sum_{l \in B} \frac{\hbar \{C_{kl}^{(1)}\}^2 [z(\omega_k) + z(\omega_l)]}{(2 m_k \omega_k)(2 m_l \omega_l)} \times \delta(\omega - \omega_k - \omega_l). \tag{16}$$

The total relaxation rate given by Eq. (12) can be divided into contributions of the phonon modes of T, R, B, and S modes, i.e.,

$$\begin{aligned} R_{\mathrm{total}} &= \sum_{k=1}^{N} R_k + \sum_{k=1}^{N} \sum_{l=1}^{N} R_{kl} \\ &= R_\alpha^T + R_\alpha^R + R_\alpha^B + R_\alpha^S + R_\beta^{TT} + R_\beta^{TR} + R_\beta^{TB} + R_\beta^{TS} \\ &\quad + R_\beta^{RR} + R_\beta^{RB} + R_\beta^{RS} + R_\beta^{BB} + R_\beta^{BS} + R_\beta^{SS}, \end{aligned} \tag{17}$$

where R_k and R_{kl} are single- and two-phonon contributions to the relaxation rate, respectively, which may be summed up together according to the frequencies to give single-phonon R_α's and two-phonon R_β's, respectively. For example, the relaxation rate by two-phonon coupling of R and B modes may be defined by

$$R_\beta^{RB} = \frac{2}{\hbar^2} \mathrm{Re}\left(\int_0^\infty ds \int_{-\infty}^{\infty} d\omega [\mathcal{T}_{\beta[1]}^{RB}(\omega) + \mathcal{T}_{\beta[1]}^{BR}(\omega) + \mathcal{T}_{\beta[2]}^{RB}(\omega) + \mathcal{T}_{\beta[2]}^{BR}(\omega)][z(\omega)\cos(\omega s) - i \sin(\omega s)] |\langle \phi_i | x | \phi_f \rangle|^2 \exp[i(\nu_i - \nu_f) s] \right). \tag{18}$$

III. RESULTS AND DISCUSSION

A. Density of states

Density of states of solvent normal modes is presented in Fig. 1. Figure 1(a) represents the normal modes for the quenched and instantaneous structures of the H_2O solution of the CN^- ion. Normal modes for the quenched structures of the D_2O solution of CN^- are shown in Fig. 1(b). From the unitary matrix elements that transfer the normal mode coordinates to the molecular coordinates, we can classify each normal mode into several types of molecular motions[72] as stated above. In Fig. 1(a), the quenched normal modes below 400 cm^{-1} and those between 400 and 1200 cm^{-1} may be assigned to molecular translations (T) and rotational librations (R), respectively.[72] In some versions of the normal mode analysis, a mode is described as a mixture of T, R, B,

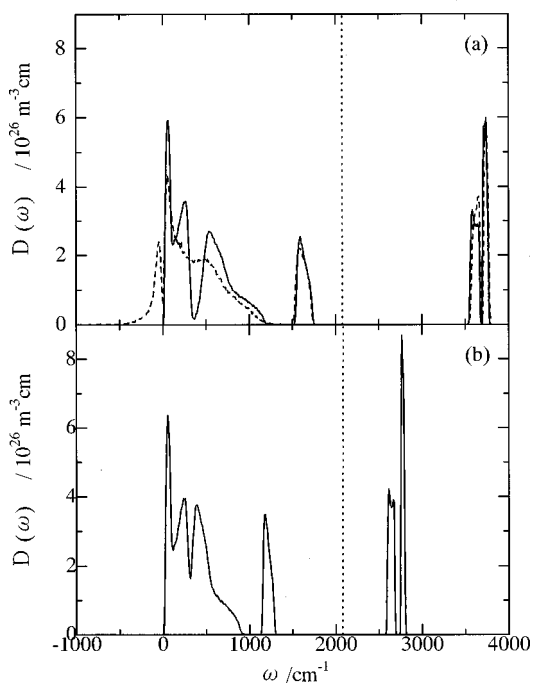

FIG. 1. The density of states $D(\omega)$ of the solvent modes calculated for (a) the quenched (solid line) and the instantaneous (dashed line) H_2O solution and (b) the quenched D_2O solution. CN^- vibrational frequency $\tilde{\omega}_s$ is about 2080 cm^{-1} (dotted line).

and *S*. However, in the present study, we follow a primitive naming of the mode.[72] Imaginary frequency modes at Im ω_k $<500\,cm^{-1}$ found for the instantaneous normal modes were excluded from the analysis. Although the band gap between *T* and *R* modes is not clear from the analysis for the instantaneous normal modes, the modes below 400 cm^{-1} and those between 400 and 1200 cm^{-1} may be referred to as *T* and *R* modes, respectively. A band found around 1600 cm^{-1} in Fig. 1(a) represents intramolecular bending (*B*) modes of H_2O molecules and doublet bands around 3700 cm^{-1} come from the intramolecular stretching (*S*) modes, i.e., symmetric and antisymmetric stretchings, of H_2O. On the other hand, for the D_2O solution in Fig. 1(b), the normal modes below 300 cm^{-1}, those between 300 and 900 cm^{-1}, those around 1200 cm^{-1}, and those around 2700 cm^{-1} represent *T*, *R*, *B*, and *S* modes, respectively. The translational and rotational modes of CN^- are found around 330 and 120 cm^{-1}, respectively. We note that these modes do not represent ''pure'' translation or rotation of CN^-. In the diagonalization of the Hessian matrix, the modes for CN^- are mixed with the *T* modes of H_2O, or *T* and *R* modes of D_2O.

The C–N vibrational frequency $\tilde{\omega}_s$ showed blue shift in the aqueous solution compared with that of the isolated CN^- ion, ω_s. The distribution of the frequency was found at $2080\,cm^{-1}<\tilde{\omega}_s<2087\,cm^{-1}$ for 30 different quenched structures in the H_2O and D_2O solution, and $2071\,cm^{-1}<\tilde{\omega}_s<2099\,cm^{-1}$ for 30 instantaneous structures in the H_2O solution.[73] The latter is a little broader than the former.

B. Coupling constants

The coupling constants between the CN^- stretching mode and the bath modes for a quenched structure of the H_2O solution are plotted in Figs. 2. In order to compare the strengths of the couplings, $C_k^{(u)}$ is multiplied by σ^u, where σ is the standard deviation of the probability that the isolated harmonic oscillator system is found at *x*,

$$\sigma=\sqrt{\langle x^2\rangle_T}=\sqrt{\hbar z(\tilde{\omega}_s)/2m_s\tilde{\omega}_s}. \tag{19}$$

In Figs. 2(a)–(c), the coupling constants linear in the bath coordinate are compared with each other. In Figs. 2(d) and 2(e), the coupling strengths of $C_{kl}^{(1)}$ and $C_{kl}^{(2)}$ are also compared. In the same manner, $C_{kl}^{(u)}$ is multiplied by $\sigma_l\sigma^u$, where

$$\sigma_l=\sqrt{\langle q_l^2\rangle_T}=\sqrt{\hbar z(\omega_l)/2m_l\omega_l}. \tag{20}$$

The scaling by σ and σ_l is reasonable because the probablity that the system is found at $x\gg\sigma$ and the bath at $q_l\gg\sigma_l$ is quite small. Thus, $C_k^{(1)}\sigma\sigma_k$, $C_k^{(2)}\sigma^2\sigma_k$, $C_k^{(3)}\sigma^3\sigma_k$, $C_{kl}^{(1)}\sigma\sigma_k\sigma_l$, and $C_k^{(2)}\sigma^2\sigma_k\sigma_l$ represent the solvent-induced potential deviation from the system potential $V_s(x)$ at $x=\sigma$, $q_k=\sigma_k$, and $q_l=\sigma_l$. The plot in each panel in Fig. 2 represents the relevant coupling constant for the 2294 bath degrees of freedom. We see that there exist various bath modes over a wide range of coupling strengths, even for a given frequency. It is found in Fig. 2 that the average of

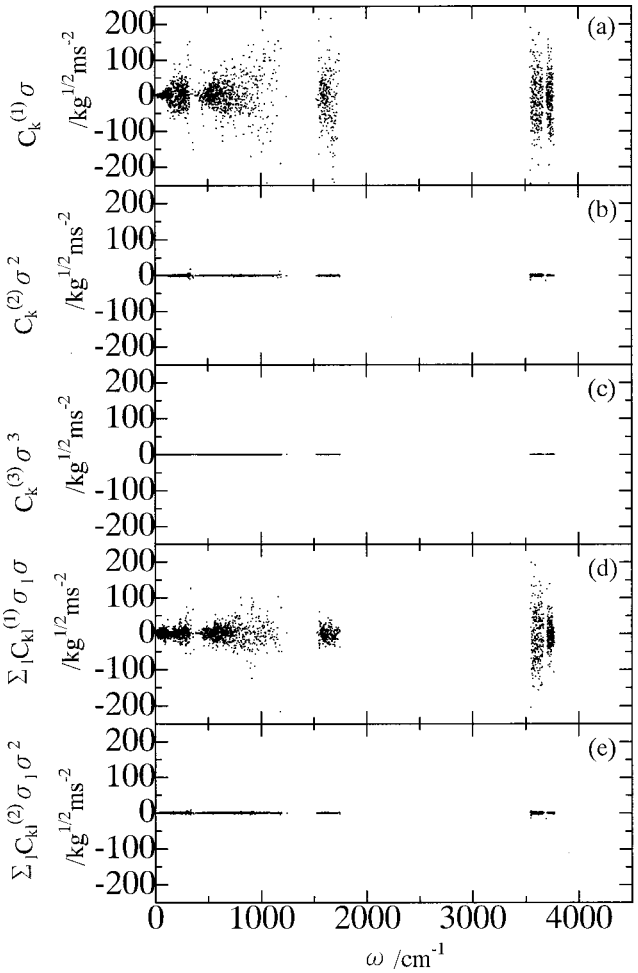

FIG. 2. Coupling constants (a) $C_k^{(1)}\sigma$, (b) $C_k^{(2)}\sigma^2$, (c) $C_k^{(3)}\sigma^3$, (d) $\Sigma_{l=1}^N C_{kl}^{(1)}\sigma_l\sigma$, and (e) $\Sigma_{l=1}^N C_{kl}^{(2)}\sigma_l\sigma^2$ for the quenched H_2O solution. For definitions, see the text.

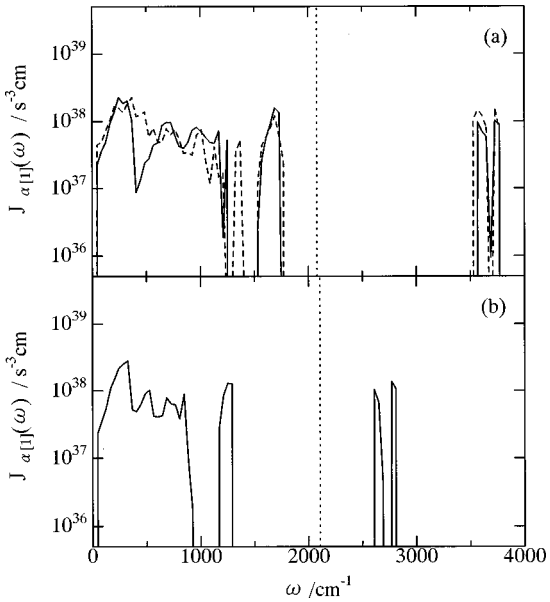

FIG. 3. Single-phonon spectral density $\mathcal{T}_{\alpha[1]}(\omega)$ calculated for (a) the quenched (solid line) and the instantaneous (dashed line) H_2O solution, and (b) the quenched D_2O solution. The dotted line at about 2080 cm^{-1} indicates the CN^- vibrational frequency.

these coupling energies seems to be zero. In other words, the coupling constant at a given frequency shows symmetric distribution with respect to its sign. Further, it is very interesting to find that the coupling strengths of $C_k^{(u)}$ and $C_{kl}^{(u)}$ become negligibly small as u becomes large. The coupling $C_k^{(1)}$ and $C_{kl}^{(1)}$, thus, have the largest contributions to the system potential among $C_k^{(u)}$'s and $C_{kl}^{(u)}$'s, respectively. This implies that it is sufficient to calculate only $C_k^{(1)}$ and $C_{kl}^{(1)}$ for the spectral densities and the relaxation time given below.

C. Spectral densities

Calculated single-phonon spectral density $\mathcal{T}_{\alpha[1]}(\omega)$ for the quenched and instantaneous normal modes of the H_2O solution is presented in Fig. 3(a). $\mathcal{T}_{\alpha[1]}(\omega)$ for the quenched D_2O solution is shown in Fig. 3(b), as well. The functions $\mathcal{T}_{\alpha[1]}(\omega)$'s averaged over 30 configurations are plotted. Within the first-order cumulant expansion of the influence functional or Fermi's golden rule, the relaxation is considered to occur as a result of the resonance between the solute mode and the solvent modes. From this viewpoint, the solute mode frequency $\tilde{\omega}_s$ must coincide with the bath mode frequency ω. However, no solvent mode is found near the CN^- vibrational frequency region around 2080 cm^{-1}, either for the H_2O or D_2O solution. This clearly indicates that the energy transfer does not occur within the single-phonon process by the linear coupling $C_k^{(1)} x q_k$. The multiphonon process plays a dominant role in the relaxation.

Two-phonon spectral densities $\mathcal{T}_{\beta[1]}(\omega)$ and $\mathcal{T}_{\beta[2]}(\omega)$ are shown in Fig. 4 for the quenched and instantaneous normal modes of the H_2O solution and quenched normal modes of the D_2O solution. The golden rule for the nonlinear coupling $C_{kl}^{(1)} x q_k q_l$ gives the resonance between the solute mode and the sum- and difference-frequency bath modes, i.e., $\omega = \omega_k \pm \omega_l$. It is clear from Figs. 4(a) and 4(b) that the sum-

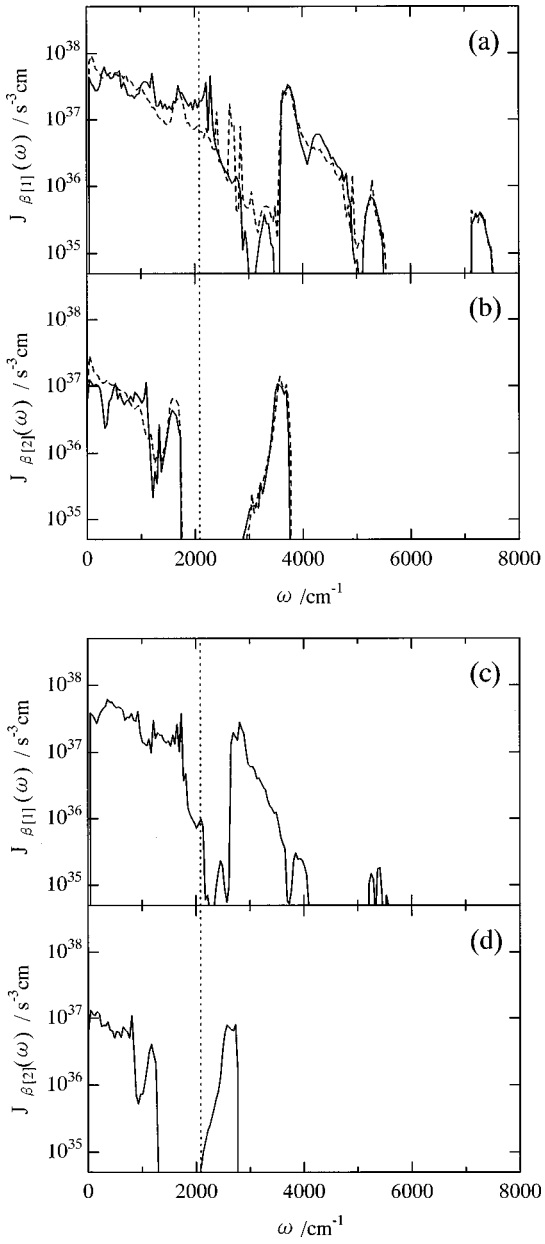

FIG. 4. Two-phonon spectral densities of $\mathcal{T}_{\beta[1]}(\omega)$, (a) and (c), and $\mathcal{T}_{\beta[2]}(\omega)$, (b) and (d), of sum- and difference-frequency modes, respectively. The solid lines in (a) and (b) represent the spectral density for the quenched H_2O solution and the dashed lines for the instantaneous H_2O solution. The solid lines in (c) and (d) are for the quenched D_2O solution. The dotted line at about 2080 cm^{-1} indicates the CN^- vibrational frequency.

frequency spectrum $\mathcal{T}_{\beta[1]}(\omega)$ of H_2O has a large value around the CN^- vibrational frequency, while practically no intensity is found there for the case of the difference-frequency spectrum $\mathcal{T}_{\beta[2]}(\omega)$. This implies that the sum-frequency process is dominant in the H_2O solution in the golden rule approximation. In Figs. 4(c) and 4(d), the sum-frequency as well as difference-frequency spectrum of the D_2O solution is found at the frequencies of the CN^- stretching frequency, although these are small compared with the sum-frequency spectrum of the H_2O solution. The relaxation rate must be much slower in the D_2O solution than in the H_2O solution.

TABLE I. Relaxation time of the vibrationally first excited state of CN^-.

System Solvation structure	CN^- in H_2O quenched	CN^- in H_2O instantaneous	CN^- in D_2O quenched
Present calculation	8 ps	7 ps	85 ps
Experiment[a]	28 ps	28 ps	71 ps

[a]Reference 13.

D. Relaxation time

In Table I, we summarize the calculated vibrational energy relaxation time T_1 of CN^- averaged over 30 different quenched and instantaneous solvation structures. In order to compare the values with the experiment, the relaxation time was calculated from the survival probability for the first excited state ϕ_1. Here, the average was made by fitting the time-dependent survival probability,

$$P(t)=\frac{1}{30}\sum_{c-1}^{30} P_c(t), \tag{21}$$

into a single exponential function $\exp(-t/T_1)$, where $P_c(t)$ is the survival probability calculated from Eq. (11) for the cth solvation structure.[74]

The averaged relaxation time T_1 for the quenched structures, 8 ps, is almost the same as that for the instantaneous structures, 7 ps. These calculated values are of the same order of magnitude as that measured by the pump-probe experiment, $T_1=28$ ps.[13] The difference may be caused by the potential functions and/or the harmonic oscillators bath approximation. Further, the relaxation time in D_2O, $T_1=85$ ps, is considerably slower than that in the H_2O solution. This isotope effect is in a good correspondence to the experiment, $T_1=28$ ps for H_2O and 71 ps for D_2O. Considering the complexity of the present process as well as the rough approximation for the potential functions, we believe that this demonstrates a reliability of the present theory.

Now, it must be reasonable to expect that the value of $P_c(t)$ is not necessarily the same among the solvation structures. To see this, the distribution of the relaxation times for 30 different solvation structures is presented in Fig. 5. Figures 5(a) and 5(b) are the results for the quenched and instantaneous structures in the H_2O solution and the quenched structures in the D_2O solution, respectively. From these figures, a large variance is found in the relaxation time among the different structures, ranging from 0 to 20 ps in the H_2O solution and 0 to 200 ps in the D_2O solution. The variance reflects the fact that the relaxation rate is fast if the solvation structure has a lot of two-phonon combinations of strongly interacting solvent modes with a C–N vibrational mode, and slow if there are few two-phonon combinations. Thus, the relaxation time depends much upon the solvation structure.

In Fig. 6, calculated time-dependent survival probabilities of different excited states are shown for the quenched H_2O solution. On the calculation of the survival probabilities of an excited state ϕ_i, an initial condition was set $\phi_i=1$ at $t=0$. The figure shows that if the system is initially at the vibrational ground state ϕ_0, it actually stay in the ground state for a very long time. The calculated relaxation times of the first, second, and third excited states were found to be 8, 4, and 2 ps, respectively. We can see from the figure that the relaxation becomes fast exponentially as the excitation becomes high.

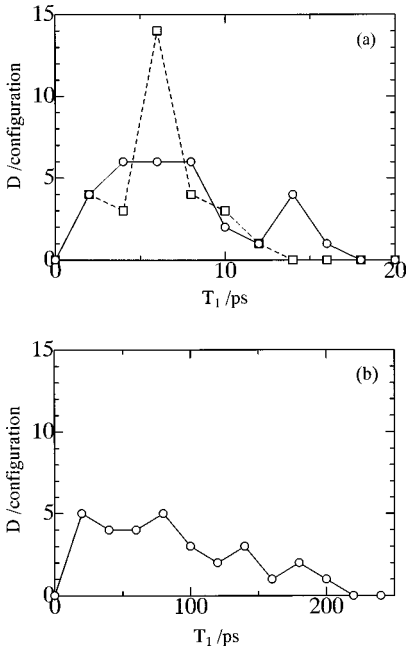

FIG. 5. The distribution of the relaxation time for 30 different (a) quenched (solid line) and instantaneous (dashed line) H_2O solutions and a (b) quenched D_2O solution. The dotted line at about 2080 cm^{-1} indicates the CN^- vibrational frequency.

Figure 7 shows the quantum effect of the solvent modes on the survival probability for the quenched H_2O solution. In the figure, a full quantum survival probability is compared with the quantum-system/classical-bath survival probability which is calculated by approximating $z(\omega_k)\approx z_c(\omega_k)$, $z(\omega_l)\approx z_c(\omega_l)$, and $z(\omega_k\pm\omega_l)\approx[1\pm z_c(\omega_k)z_c(\omega_l)]/[z_c(\omega_k)\pm z_c(\omega_l)]$ for Eqs. (13) and (14), where $z_c(\omega)=(\beta\hbar\omega/2)^{-1}$ is the classical approximation of $z(\omega)$. This approximation is essentially the same as the one that has been widely made on the evaluation of the relaxation rate using the classical force–force autocorrelation function. The function may easily be obtained from the time evolution of the classical force exerted on the C–N axis by conventional classical MD calculations. However, the classical-bath relax-

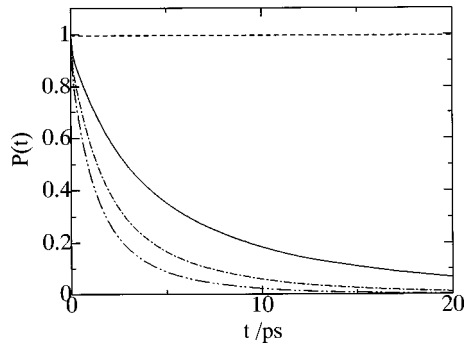

FIG. 6. Time-dependent survival probabilities of vibrational ground state ϕ_0 (dashed line), and excited states ϕ_1 (solid line), ϕ_2 (single dotted–dashed line), and ϕ_3 (double dotted–dashed line) calculated for the quenched H_2O solution. The plots show averaged probabilities $P(t)$ in Eq. (21).

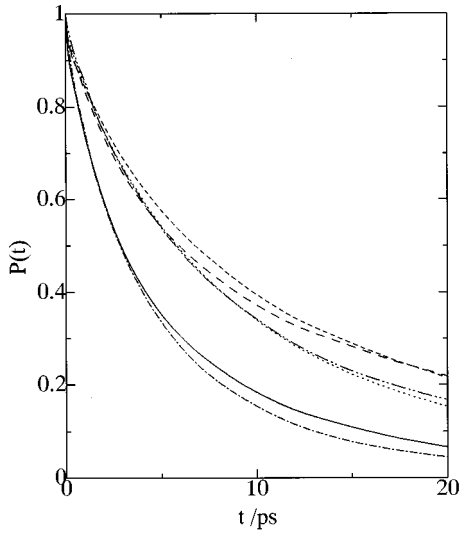

FIG. 7. Quantum-system/quantum-bath survival probability calculated for the quenched (solid line) and instantaneous (single dotted–dashed line) H_2O solution, the quantum-system/classical-bath survival probability calculated for the quenched (long dashed line) and the instantaneous (double dotted–dashed line) H_2O solution, and the survival probability of the system in the classical bath with quantum correction calculated for the quenched (short dashed line) and the instantaneous (dotted line) H_2O solution. The plots show averaged probabilities $P(t)$ in Eq. (21).

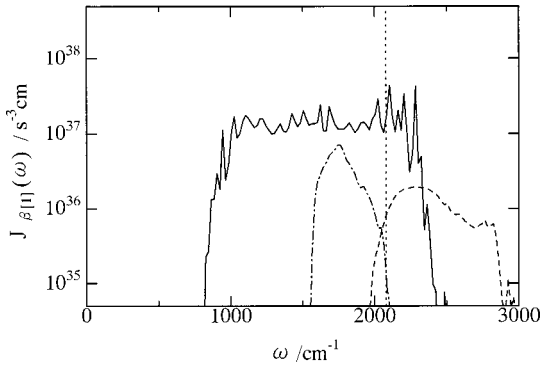

FIG. 8. Partial sum-frequency spectral densities for RR sum-frequency modes $\mathcal{T}^{RR}_{\beta[1]}(\omega)$ (solid line), RB sum-frequency modes $\mathcal{T}^{RB}_{\beta[1]}(\omega)$ (dashed line), and TB sum-frequency modes $\mathcal{T}^{TB}_{\beta[1]}(\omega)$ (dotted–dashed line) for the quenched H_2O solution.

ation time was found to be about two times longer than the quantum-bath relaxation time. Thus, the classical approximation largely underestimates the vibrational energy relaxation rate approximately by a factor of 2.

Recently, a quantum correction has been made, as proposed by Bader and Berne,[45] by multiplying the spectrum of the correlation function by $z(\omega)/z_c(\omega)=(\beta\hbar\omega/2)\times\coth(\beta\hbar\omega/2)$. This must be valid for the case of the single-phonon process. Rigorously speaking, however, it is not correct for the multiphonon processes.[3,49,54] Now, it is interesting to test this quantum corrections based upon the present spectra. The survival probability of the quantum system in the classical bath with the quantum correction was evaluated by approximating $z(\omega_k)\approx z_c(\omega_k)$ and $z(\omega_l)\approx z_c(\omega_l)$ in Eq. (14), leaving $z(\omega_k\pm\omega_l)$ unchanged in Eq. (13). The result is given in Fig. 7, where the approximated survival probabilities $P(t)$ are compared with the fully quantum one. It is clear from the figure that the quantum correction for the classical bath improves little the survival probability or the relaxation time for the present system.

E. Analysis of bath modes

As clearly shown above, the two-phonon coupling plays the dominant role in the vibrational relaxation process of the present system. Now, it is interesting to investigate the bath mode pairs that have large contributions to the relaxation. To do this, partial sum-frequency spectral densities as defined by Eq. (16) were evaluated. The result for the quenched H_2O solution, for example, is presented in Fig. 8. It is found from this figure that, in the H_2O solution, sum-frequency modes composed of two rotational libration modes [RR sum-frequency spectral density $\mathcal{T}^{RR}_{\beta[1]}(\omega)$[75]] is dominant. The spectral density composed of rotational libration and intramolecular bending modes [RB sum-frequency spectral density $\mathcal{T}^{RB}_{\beta[1]}(\omega)$] is small at the C–N vibrational frequency region. However, TB sum-frequency spectral density shows a nonzero but negligibly small value there. Other contributions such as TT, TR, TS, RS, BB, BS, and SS are all zero. Thus, the translation libration mode shows no contribution to the relaxation in the quenched H_2O solution since all the contributions from TT, TR, TB, and TS are zero. The intramolecular stretching mode has no contribution, either, in the quenched H_2O solution, since TS, RS, BS, and SS contributions are all zero.

Further, Fig. 9 presents a two-dimensional analysis of R_{kl}, i.e., the contribution of two normal modes to the relaxation rate. Figures 9(a), 9(b), and 9(c) show R_{kl} as a function of two-phonon frequencies ω_k and ω_l for the quenched and instantaneous configurations of the H_2O solution, and the quenched configurations of the D_2O solution, respectively. The averaged values over 30 different configurations are presented in these figures. Peaks are found, as expected, in the region where the sum frequency of two bath phonons is very similar to the C–N vibrational frequency, i.e., $\omega_s=\omega_k+\omega_l$. Clearly, Figs. 9(a) and 9(b) indicate that the relaxation process in the H_2O solution is dominated by the sum-frequency coupling of two rotational libration modes, where $900\,\mathrm{cm}^{-1}<\omega_k<1200\,\mathrm{cm}^{-1}$ and $900\,\mathrm{cm}^{-1}<\omega_l<1200\,\mathrm{cm}^{-1}$, and the sum-frequency coupling of the bending mode and the rotational libration mode, where $1500\,\mathrm{cm}^{-1}<\omega_k<1700\,\mathrm{cm}^{-1}$ and $400\,\mathrm{cm}^{-1}<\omega_l<600\,\mathrm{cm}^{-1}$, respectively. These have qualitatively been demonstrated already by the partial spectral density presented in Fig. 8. On the other hand, the contribution from the translational motion of H_2O molecules ($\omega_k<400\,\mathrm{cm}^{-1}$ or $\omega_l<400\,\mathrm{cm}^{-1}$) is negligibly small. Further, the contribution of the CN^- translational mode (around 330 cm^{-1}) and the rotational mode (around 120 cm^{-1}), which are mostly coupled to the translational motion of H_2O molecules, are very small. On the other hand, the relaxation process in the D_2O solution is found to be dominated by sum-frequency coupling of the bending mode and the rotational libration mode, where $1200\,\mathrm{cm}^{-1}<\omega_k<1300\,\mathrm{cm}^{-1}$ and $800\,\mathrm{cm}^{-1}<\omega_l<900\,\mathrm{cm}^{-1}$. Further, it is interesting to find some peaks at the locations where the difference frequency of two bath

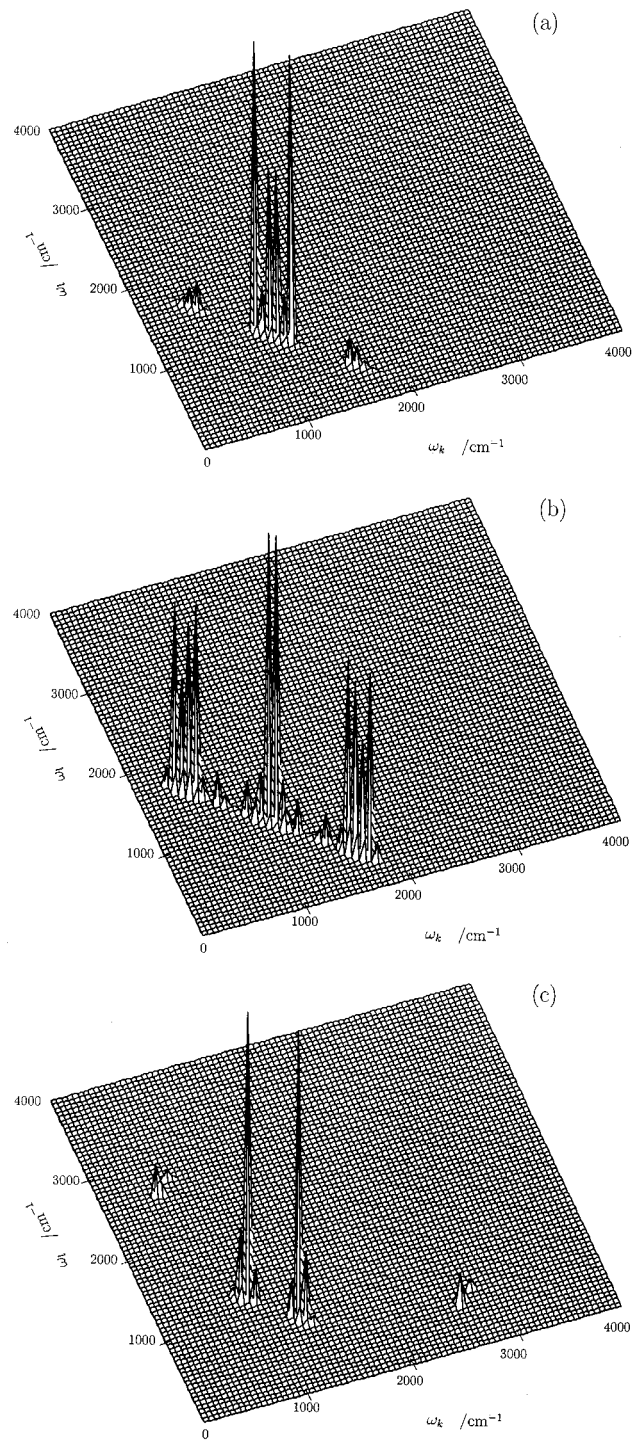

FIG. 9. The two-dimensional frequency distribution of R_{kl} calculated for (a) the quenched H_2O solution, (b) the instantaneous H_2O solution, and (c) the quenched D_2O solution.

phonons is almost the same as C–N vibrational frequency, i.e., $|\omega_k-\omega_l|=\omega_s$. Thus, the difference-frequency coupling of the stretching mode and the rotational libration mode, where $2600\,\mathrm{cm}^{-1}<\omega_k<2800\,\mathrm{cm}^{-1}$ and $500\,\mathrm{cm}^{-1}<\omega_l<700\,\mathrm{cm}^{-1}$, respectively, has a contribution to the relaxation to some extent, too. However, the contribution of the CN^- rotational or translational mode, which is coupled to the translational and rotational motion of D_2O molecules, respectively, contributes little in the relaxation process.

TABLE II. Contributions from various pairs of bath modes to the vibrational relaxation.

System Solvation structure	CN^- in H_2O quenched	CN^- in H_2O instantaneous	CN^- in D_2O quenched
TT	0%	0%	0%
TR	0%	0%	0%
TB	0%	18%	0%
TS	0%	0%	0%
RR	88%	34%	0%
RB	12%	48%	80%
RS	0%	0%	20%
BB	0%	0%	0%
BS	0%	0%	0%
SS	0%	0%	0%

The intensities of the diagonal coupling constants C_{kk} are found not to be overwhelmingly strong compared to those of the nondiagonal ones, C_{kl}. Further, the number of $C_{kk}\,(=N)$ is smaller than that of $C_{kl}\,(=N^2-N)$. Thus, most contributions are from the nondiagonal couplings. In other words, the multiphonon coupling of different phonons k and l is essential for the present system.

Contributions of each pair of the bath mode types to the relaxation rate are listed in Table II. We must note here that the instantaneous and quenched structures have different fractions, although it is not clear which approximation is better to describe the vibrational relaxation. This may come from the difference in the density of states between instantaneous and quenched normal modes shown in Figs. 1(a) and 1(b). We could not reach a conclusion here as to whether the H_2O bending mode is significant in the relaxation process or not. Experiments that can detect the excitation of H_2O bending might help to answer this question.

Pictures of typical two bath modes that have a great contribution to the relaxation in the H_2O solution for the quenched structure is shown in Fig. 10. These are the two rotational libration modes, $\omega_k=900\,\mathrm{cm}^{-1}$ and $\omega_l=1186\,\mathrm{cm}^{-1}$, which give the largest value of R_{kl} among all pairs of the bath modes k and l in a quenched solvation structure in H_2O, where $\tilde{\omega}_s=2086\,\mathrm{cm}^{-1}$. We can see from the figure that the normal mode coordinate is delocalized in space. In some papers,[63–65] individual motion of the molecules in the modes have been explored to understand how it influences the solute in relation to the relaxation process. Here, in order to extract important molecular motions from the bath modes, we picked up 100 bath mode pairs that give large values of R_{kl} from each solvation structure. Figure 11(a) shows the ''motion'' $\Delta(r)$ for these bath modes as a function of distance from the CN^- ion, where the motion $\Delta(r)$ was defined by

$$\Delta(r)=\langle\Delta\mathrm{H}_1(r)+\Delta\mathrm{H}_2(r)+\Delta\mathrm{O}(r)\rangle, \tag{22}$$

where $\Delta\mathrm{H}_1(r)$, $\Delta\mathrm{H}_2(r)$, and $\Delta\mathrm{O}(r)$ are the root square displacement of two H atoms and O atom of water, whose center of mass is located at r from the CN^- ion in Cartesian coordinates caused by the oscillation of the corresponding normal mode coordinate by $\pm\sigma_k$. The average $\langle\cdots\rangle$ was taken over the 3000 bath modes.

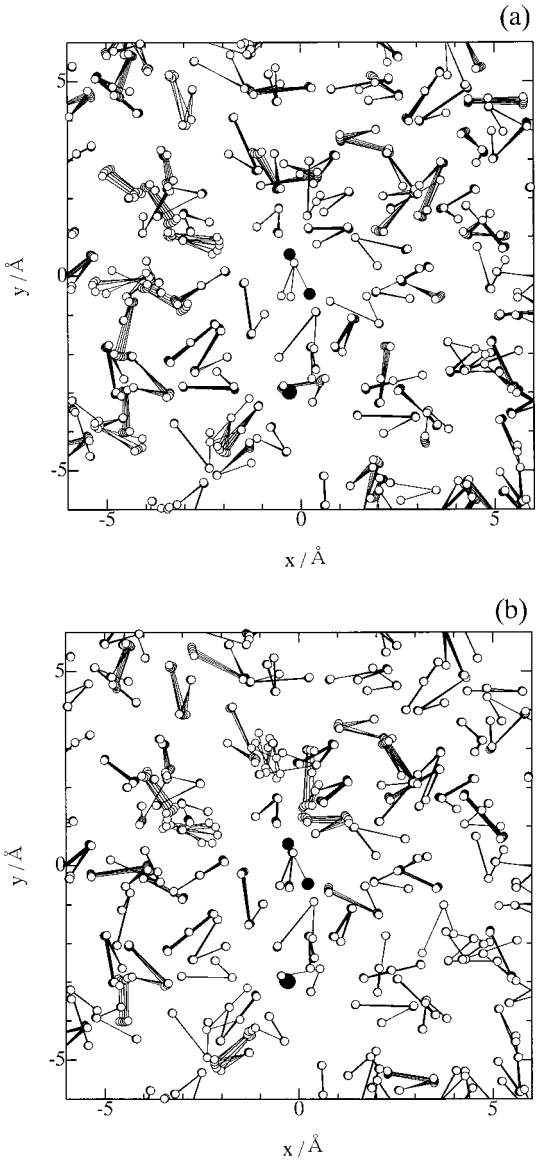

FIG. 10. Snapshots of the two solvent modes, (a) the rotational libration mode at $\omega_k = 900\,\mathrm{cm}^{-1}$ and (b) The rotational libration mode at $\omega_l = 1186\,\mathrm{cm}^{-1}$, found in a quenched structure of the H_2O solution. The combination of these two solvent modes gives the largest R_{kl} value. The white circles represent H and O atoms of the solvent H_2O, the black circles represent C and N atoms of CN^-, and a large black circle represents Na^+. Each picture shows a superposition of five snapshots, where displacement of the atoms represents a fluctuation of the normal mode coordinates.

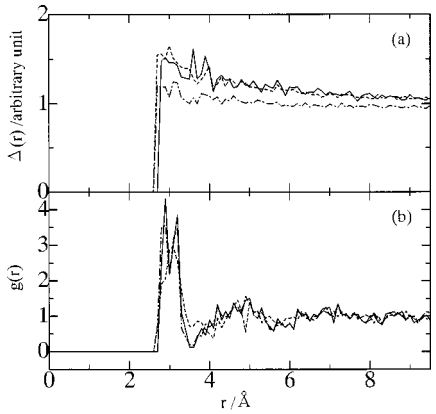

FIG. 11. (a) The motion of solvent modes $\Delta(r)$ and (b) radial distribution function $g(r)$ between the CN^- ion and water molecules calculated for the quenched H_2O solution (solid line), the instantaneous H_2O solution (dashed line), and the quenched D_2O solution (dotted–dashed line).

Comparing $\Delta(r)$ with the radial distribution function $g(r)$ between the center of masses of the cyanide ion and water molecules shown in Fig. 11(b), we can find that the water molecules near the CN^- ion have strong motions. Motions of water molecules beyond the second solvation shell become a little weak, although the change is rather slow.

IV. CONCLUSION

In the present paper, we showed a successful application of the influence of functional theory combined with the normal mode analysis to vibrational energy relaxation in the solution.

There are two major factors of the solvent modes that determine the vibrational relaxation rate. The first is the frequency match between the solute and the solvent modes. When there are no solvent modes whose frequencies are equal to $\tilde{\omega}_s$ or $u\tilde{\omega}_s$, the multiphonon process becomes important. In this case the sum- and difference-frequency combinations of this process becomes important. In this case the sum- and difference-frequency combinations of solvent phonons $\omega_k \pm \omega_l \pm \cdots$ must match $\tilde{\omega}_s$ or $u\tilde{\omega}_s$. Second, the coupling constants of the solvent modes, which satisfy the frequency matching condition above, must be large for the single-phonon and multiphonon processes. These two conditions have to be satisfied simultaneously for the vibrational relaxation rate to be fast. In the present study, two conditions were tested by single- and two-phonon spectral densities in Figs. 3 and 4. As clearly shown in the figures, vibrational relaxation of the CN^- ion in the aqueous solutions is found to be caused mainly by the two-phonon process. The resultant relaxation time was in moderate agreement with the experiment. The solvent isotope effect was in good correspondence to the experiment, as well. Analyzing the solvent modes that satisfy these conditions, we are able to see what sorts of molecular motions contribute to the relaxation and what sorts of modes do not. In the H_2O solution, the coupling between two R modes and the one between R and B modes are significant. In the D_2O solution, the coupling between R and B modes and the coupling between R and S modes contribute much to the relaxation. The reason why the relaxation in the D_2O solution is slower than that in H_2O is that the frequency matching is not favorably satisfied since the deutron atoms cause the frequency shift to smaller ω of the density of states, as shown in Fig. 1. It is found, too, that the phonons that represent active motions of water molecules close to the CN^- ion are particularly important for the relaxation.

Finally, a more precise approximation for the evaluation of the relaxation rate may be available along this line, based upon the exact path integration for the present second-order perturbative influence functional.[3] This gives an evaluation

of the contribution of higher-order perturbation terms than Fermi's golden rule to the relaxation.

ACKNOWLEDGMENTS

The authors thank the computer centers of the Institute for Molecular Science, Tokyo Institute of Technology, and the Japan Atomic Energy Research Institute for the use of supercomputers. The work was supported in part by a Grant-in-Aid for Scientific Research (No. 09440197 and No. 11166222) from the Ministry of Education, Science, and Culture, Japan.

[1] R. P. Feynman and F. L. Vernon, Ann. Phys. (N.Y.) **24**, 118 (1963).
[2] R. P. Feynman and A. R. Hibbs, *Quantum Mechanics and Path Integrals* (McGraw-Hill, New York, 1965).
[3] M. Shiga and S. Okazaki, J. Chem. Phys. **109**, 3542 (1998).
[4] M. Shiga and S. Okazaki, Chem. Phys. Lett. **292**, 431 (1998).
[5] A. Laubereau and W. Kaiser, Rev. Mod. Phys. **50**, 607 (1978).
[6] E. J. Heilweil, M. P. Casassa, R. R. Cavanagh, and J. C. Stephenson, Annu. Rev. Phys. Chem. **40**, 143 (1989).
[7] T. Elsaesser and W. Kaiser, Annu. Rev. Phys. Chem. **42**, 83 (1991).
[8] *Applied Laser Spectroscopy*, edited by D. L. Abdrews (VCH, New York, 1992).
[9] *Activated Barrier Crossing*, edited by G. R. Flemming and P. Hänggi (World Scientific, River Edge, 1993).
[10] *Ultrashort Laser Pulses*, edited by A. Kaiser (Springer-Verlag, New York, 1993).
[11] J. C. Owrutsky, D. Raftery, and R. M. Hochstrasser, Annu. Rev. Phys. Chem. **45**, 519 (1994).
[12] E. J. Heilweil, F. E. Doany, R. Moore, and R. M. Hochstrasser, J. Chem. Phys. **76**, 5632 (1982).
[13] P. Hamm, M. Lim, and R. M. Hochstrasser, J. Chem. Phys. **107**, 10 523 (1997).
[14] F. K. Fong, S. L. Naberhuis, and M. M. Miller, J. Chem. Phys. **56**, 4020 (1972).
[15] W. E. Hagston and J. E. Lowther, Physica (Amsterdam) **70**, 40 (1973).
[16] S. H. Lin, J. Chem. Phys. **61**, 3810 (1974).
[17] D. J. Diestler, J. Chem. Phys. **60**, 2692 (1974).
[18] A. Nitzan and R. J. Silbey, J. Chem. Phys. **60**, 4070 (1974).
[19] A. Nitzan, S. Mukamel, and J. Jortner, J. Chem. Phys. **60**, 3929 (1974).
[20] A. Nitzan, S. Mukamel, and J. Jortner, J. Chem. Phys. **63**, 200 (1975).
[21] J. Jortner, Mol. Phys. **32**, 379 (1976).
[22] S. H. Lin, J. Chem. Phys. **64**, 441 (1976).
[23] S. H. Lin, J. Chem. Phys. **65**, 1053 (1976).
[24] *Radiationless Processes in Molecules and Condensed Phases*, edited by F. K. Fong (Springer-Verlag, Berlin, 1976).
[25] Y. Weissman, A. Nitzan, and J. Jortner, Chem. Phys. **26**, 413 (1977).
[26] D. W. Oxtoby, Adv. Chem. Phys. **40**, 1 (1979).
[27] D. W. Oxtoby, Adv. Chem. Phys. **47**, 487 (1981).
[28] D. W. Oxtoby, Annu. Rev. Phys. Chem. **32**, 77 (1981).
[29] K. K. Pukhov and V. P. Sakun, Phys. Status Solidi B **95**, 391 (1979).
[30] *Radiationless Transitions*, edited by S. H. Lin (Academic, New York, 1980).
[31] *Intramolecular Dynamics*, edited by J. Jortner and B. Pullman (Reidel, Dordrecht, 1982).
[32] W. G. Rothschild, *Dynamics of Molecular Liquids* (Wiley, New York, 1984).
[33] B. N. J. Persson, J. Phys. C **17**, 4741 (1984).
[34] P. S. Dardi and R. I. Cukier, J. Chem. Phys. **86**, 2264 (1987).
[35] Z. Bao-zheng, L. Yu-xin, L. Mei-rong, and C. Wen-ju, Chin. Phys. **10**, 876 (1990).
[36] R. M. Whitnell, K. R. Wilson, and J. T. Hynes, J. Chem. Phys. **94**, 8625 (1990).
[37] R. M. Whitnell, K. R. Wilson, and J. T. Hynes, J. Chem. Phys. **96**, 5354 (1992).
[38] M. Topaler and N. Makri, J. Chem. Phys. **97**, 9001 (1992).
[39] F. E. Figueirido and R. M. Levy, J. Chem. Phys. **97**, 703 (1992).
[40] M. Tuckerman and B. J. Berne, J. Chem. Phys. **98**, 7301 (1993).
[41] H. Gai and G. A. Voth, J. Chem. Phys. **99**, 740 (1993).
[42] A. S. Adelman, R. H. Stote, and R. Muralidhar, J. Chem. Phys. **99**, 1320 (1993).
[43] A. S. Adelman, R. Muralidhar, and R. H. Stote, J. Chem. Phys. **99**, 1333 (1993).
[44] Y. C. Sun, H. Gai, and G. A. Voth, Chem. Phys. **205**, 11 (1996).
[45] J. S. Bader and B. J. Berne, J. Chem. Phys. **100**, 8359 (1994).
[46] V. M. Kenkre, A. Tokmakoff, and M. D. Fayer, J. Chem. Phys. **101**, 10 618 (1994).
[47] S. Mukamel, *Principles of Nonlinear Optical Spectroscopy* (Oxford University Press, New York, 1995).
[48] B. Mishra and B. J. Berne, J. Chem. Phys. **103**, 1160 (1995).
[49] S. A. Egorov and J. L. Skinner, J. Chem. Phys. **103**, 1533 (1995).
[50] S. A. Egorov and J. L. Skinner, J. Chem. Phys. **105**, 7047 (1996).
[51] S. A. Egorov and J. L. Skinner, J. Chem. Phys. **105**, 10 153 (1996).
[52] S. A. Egorov and J. L. Skinner, J. Chem. Phys. **106**, 1034 (1997).
[53] J. S. Bader, B. J. Berne, E. Pollak, and P. Hänggi, J. Chem. Phys. **104**, 1111 (1996).
[54] S. A. Egorov and B. J. Berne, J. Chem. Phys. **107**, 6050 (1997).
[55] R. Rey and J. T. Hynes, J. Chem. Phys. **104**, 2356 (1996).
[56] R. Rey and J. T. Hynes, J. Chem. Phys. **108**, 142 (1998).
[57] S. J. Schvaneveldt and R. F. Loring, J. Chem. Phys. **102**, 2326 (1995).
[58] S. J. Schvaneveldt and R. F. Loring, J. Chem. Phys. **104**, 4736 (1996).
[59] S. J. Schvaneveldt and R. F. Loring, J. Phys. Chem. **100**, 10 355 (1996).
[60] G. Goodyear, R. E. Larsen, and R. M. Stratt, Phys. Rev. Lett. **76**, 243 (1996).
[61] G. Goodyear and R. M. Stratt, J. Chem. Phys. **105**, 10 050 (1996).
[62] G. Goodyear and R. M. Stratt, J. Chem. Phys. **107**, 3098 (1997).
[63] R. E. Larsen, E. F. David, G. Goodyear, and R. M. Stratt, J. Chem. Phys. **107**, 524 (1997).
[64] B. M. Ladanyi and R. M. Stratt, J. Phys. Chem. A **102**, 1068 (1998).
[65] R. E. Larsen and R. M. Stratt, J. Chem. Phys. **110**, 1036 (1999).
[66] G. Gershinsky and E. Pollak, J. Chem. Phys. **101**, 7174 (1994).
[67] G. Gershinsky and E. Pollak, J. Chem. Phys. **103**, 8501 (1995).
[68] J. Cao and G. A. Voth, J. Chem. Phys. **103**, 4211 (1995).
[69] M. Ferrario, I. R. McDonald, and M. L. Klein, J. Chem. Phys. **84**, 3975 (1986).
[70] W. L. Jorgensen, J. Chandrasekhar, J. D. Madura, R. W. Impey, and M. L. Klein, J. Chem. Phys. **79**, 926 (1983).
[71] A. O. Caldeira and A. J. Leggett, Physica A **121**, 587 (1983).
[72] A. Pohorille, L. R. Pratt, R. A. LaViolette, M. A. Wilson, and R. D. MacElroy, J. Chem. Phys. **87**, 6070 (1987).
[73] M. Shiga and S. Okazaki, Mol. Simul. **21**, 377 (1999).
[74] Since semi-log plot of $P(t)$ shows a linear line only at t larger than several pico seconds, the fitting was done for this exponential region. Summation of exponential functions, i.e., Eq. (21), is, in general, not an exponential function.
[75] Superscript *RR* represents a combination of two rotational libration modes in sum- and difference-spectral densities. This does not mean a mixture of two modes in a normal mode which is sometimes used to understand actual molecular motions in the mode. See M. Buchner, B. M. Ladanyi, and R. M. Stratt, J. Chem. Phys. **97**, 8522 (1992).